

# UC Berkeley

## UC Berkeley Previously Published Works

### Title

Towards a universal model for carbon dioxide uptake by plants

### Permalink

<https://escholarship.org/uc/item/43r3t96n>

### Journal

Nature Plants, 3(9)

### ISSN

2055-026X

### Authors

Wang, Han  
Prentice, I Colin  
Keenan, Trevor F  
[et al.](#)

### Publication Date

2017-09-01

### DOI

10.1038/s41477-017-0006-8

Peer reviewed

1 ***Title:***

2

3 **Towards a universal model for carbon dioxide uptake by plants**

4

5 ***Authors:***

6

7 Han Wang<sup>1,2,3\*</sup>, I. Colin Prentice<sup>1,2,4</sup>, Trevor F. Keenan<sup>2,5</sup>, Tyler W. Davis<sup>4,6</sup>, Ian J. Wright<sup>2</sup>, William K.  
8 Cornwell<sup>7</sup>, Bradley J. Evans<sup>2,8</sup> and Changhui Peng<sup>1,9\*</sup>

9

10 ***Affiliations:***

11 <sup>1</sup> State Key Laboratory of Soil Erosion and Dryland Farming on the Loess Plateau, College of Forestry,  
12 Northwest A & F University, Yangling 712100, Shaanxi, China

13 <sup>2</sup> Department of Biological Sciences, Macquarie University, North Ryde, NSW 2109, Australia

14 <sup>3</sup> Ecosystems Services and Management Program, International Institute for Applied Systems Analysis,  
15 Laxenburg, A-2361, Austria

16 <sup>4</sup> AXA Chair of Biosphere and Climate Impacts, Department of Life Sciences, Imperial College  
17 London, Silwood Park Campus, Buckhurst Road, Ascot SL5 7PY, UK

18 <sup>5</sup> Earth Sciences Division, Lawrence Berkeley National Laboratory, 1 Cyclotron Road, Berkeley, CA  
19 94720, United States

20 <sup>6</sup> United States Department of Agriculture-Agricultural Research Service, Robert W. Holley Center for  
21 Agriculture and Health, Ithaca, NY 14853, United States

22 <sup>7</sup> Ecology and Evolution Research Centre, School of Biological, Earth and Environmental Sciences,  
23 The University of New South Wales, Randwick, NSW 2052, Australia

24 <sup>8</sup> Faculty of Agriculture and Environment, Department of Environmental Sciences, The University of  
25 Sydney, NSW 2006, Australia

26 <sup>9</sup> Department of Biological Sciences, Institute of Environmental Sciences, University of Quebec at  
27 Montreal, C.P. 8888, Succ. Centre-Ville, Montréal H3C 3P8, Québec, Canada

28

29 ***Manuscript type:*** Letter

30

31 ***\*Correspondence to:***

32 H Wang: wanghan\_sci@yahoo.com, C Peng: peng.changhui@uqam.ca

34 **Gross primary production (GPP) – the uptake of CO<sub>2</sub> by leaves, and its conversion to sugars by**  
35 **photosynthesis – is the basis for life on land. Earth System Models (ESMs) incorporating the**  
36 **interactions of land ecosystems and climate are used to predict the future of the terrestrial sink**  
37 **for anthropogenic carbon dioxide (CO<sub>2</sub>)<sup>1</sup>. ESMs require accurate representation of GPP. But**  
38 **current ESMs disagree on how GPP responds to environmental variations<sup>1,2</sup>, suggesting a need**  
39 **for a more robust theoretical framework for modelling<sup>3,4</sup>. Here we focus on a key quantity for**  
40 **GPP, the ratio of leaf-internal to external CO<sub>2</sub> ( $\chi$ ).  $\chi$  is tightly regulated and depends on**  
41 **environmental conditions, but is represented empirically and incompletely in today’s models. We**  
42 **show that a simple evolutionary optimality hypothesis<sup>5,6</sup> predicts specific quantitative**  
43 **dependencies of  $\chi$  on temperature, vapour pressure deficit and elevation; and that these same**  
44 **dependencies emerge from an independent analysis of empirical  $\chi$  values, derived from a**  
45 **worldwide data set of > 3500 leaf stable carbon isotope measurements. A single global equation**  
46 **embodying these relationships then unifies the empirical light use efficiency (LUE) model<sup>7</sup> with**  
47 **the standard model of C<sub>3</sub> photosynthesis<sup>8</sup>, and successfully predicts GPP measured at eddy-**  
48 **covariance flux sites. This success is notable given the equation’s simplicity and broad**  
49 **applicability across biomes and plant functional types. It provides a theoretical underpinning for**  
50 **the analysis of plant functional co-ordination across species and emergent properties of**  
51 **ecosystems, and a potential basis for the reformulation of the controls of GPP in next-generation**  
52 **ESMs.**

53 The standard model<sup>8</sup> accurately describes the instantaneous environmental and physiological controls  
54 of photosynthesis, whereas empirical LUE models can predict primary production over weeks to  
55 months<sup>7,9</sup> (Supplementary Information). The connection between these parallel modelling frameworks  
56 remains unresolved<sup>9</sup>. Both require independent information to be provided: leaf-internal CO<sub>2</sub> partial  
57 pressure ( $c_i$ ) and photosynthetic capacities for carboxylation and electron transport ( $V_{cmax}$  and  $J_{max}$ ) in  
58 the Farquhar model, and environmental response functions in LUE models. There is no accepted  
59 general way to do this for large-scale modelling<sup>10,11</sup>, and as a result, different implementations of  
60 apparently the same model can give very different answers in different ESMs.

61 The biochemical reactions of photosynthesis depend on the value of  $c_i$ <sup>8,12</sup>. CO<sub>2</sub> diffuses into  
62 leaves through the stomata (microscopic pores in the leaf surface) towards the chloroplasts, where  
63 reducing power derived from solar energy is used to assimilate CO<sub>2</sub> into organic forms through the  
64 Calvin cycle. The term  $c_i$  refers to the partial pressure of CO<sub>2</sub> in the intercellular space, which is lower  
65 than the ambient CO<sub>2</sub> partial pressure ( $c_a$ ) while photosynthesis is active due to the resistance imposed  
66 by the stomata. The term  $c_c$  (applying at the chloroplasts, where carbon fixation occurs) is generally  
67 even smaller than  $c_i$  due to additional resistance to CO<sub>2</sub> transport in the mesophyll (a point that we  
68 return to later) but most current models disregard this additional drawdown of CO<sub>2</sub>. Thus, given  
69 knowledge of  $c_a$ , the quantity  $\chi = c_i/c_a$  becomes a key modelling target.  $\chi$  is tightly regulated by the fast  
70 (time scale of minutes) responses of both photosynthetic rate and stomatal aperture to environmental  
71 fluctuations. However, current stomatal models used in ESMs account only for the response of  $\chi$  to

72 moisture, represented by empirical and non-equivalent formulations<sup>13</sup>, while satellite-based products  
73 based on LUE do not represent  $c_i$  at all (Supplementary Information). We propose that a firm basis for  
74 the prediction of  $\chi$  is an essential first step towards a first-principles representation of terrestrial plant  
75 carbon uptake.

76 Long-term effective values of  $\chi$  can be reconstructed from data on leaf stable carbon isotope  
77 ratios ( $\delta^{13}\text{C}$ ). Previous analyses of leaf  $\delta^{13}\text{C}$  data have examined relationships with environmental  
78 factors statistically, with many using leaf  $\delta^{13}\text{C}$  as a palaeoclimatic indicator of moisture-related climate  
79 variables only<sup>14</sup>. Here we predict the environmental responses of  $\chi$  theoretically, reserving the leaf  $\delta^{13}\text{C}$   
80 measurements for testing. Our theoretical approach depends on the idea of evolutionary optimality in  
81 balancing the costs of water loss and carbon gain – a long-standing source of hypotheses to account for  
82 stomatal behavior<sup>15,16</sup>. We derive theoretical dependencies of ‘optimal’  $\chi$  (termed  $\chi_o$ ) on growing-  
83 season air temperature, vapour pressure deficit, and elevation above sea level based on the least-cost  
84 hypothesis<sup>5,6</sup>, which states that plants minimize the combined costs of maintaining the capacities for  
85 carboxylation (maintaining the activity of Rubisco, the primary carboxylating enzyme, and other  
86 photosynthetic proteins) and transpiration (maintaining living tissues to support water transport)  
87 required to achieve a given assimilation rate. We derive effective growing-season values of  $\chi$  from a  
88 large global compilation of  $\delta^{13}\text{C}$  measurements on leaves of  $\text{C}_3$  plants<sup>17</sup> (Supplementary Figure 1) with  
89 a standard method<sup>18</sup>, and use these values to test the theory’s predictions. We then invoke the  
90 hypothesis of co-limitation between carboxylation- and electron transport-limited photosynthetic rates  
91 to provide a universal model of GPP in  $\text{C}_3$  plants, which is shown to unify the Farquhar and LUE  
92 models for  $\text{C}_3$  photosynthesis. Finally the model is tested against GPP data derived from eddy-  
93 covariance flux measurements.

94 The theory developed in Methods predicts that the quantity logit ( $\chi_o$ ) =  $\ln [\chi_o / (1 - \chi_o)]$  should  
95 rise with growth temperature ( $T_g$ ) by  $\sim 0.0545$  per Kelvin due to increased assimilation costs (the  
96 affinity of Rubisco for  $\text{CO}_2$  versus  $\text{O}_2$  declines with temperature) and reduced water transport costs (the  
97 viscosity of water declines). Due to the increase in transpiration costs imposed by increasing vapour  
98 pressure deficit (vpd), logit ( $\chi_o$ ) also should fall by 0.5 per unit increase of natural log transformed  $D_0$   
99 (the vpd that would be obtained at standard atmospheric pressure under the same temperature and  $\text{H}_2\text{O}$   
100 mole fraction). With increasing elevation the saturated vapour pressure of water remains constant while  
101 the actual vapour pressure (all other factors constant) declines, implying increased transpiration costs;  
102 while the partial pressure of  $\text{O}_2$  also declines, increasing the affinity of Rubisco for  $\text{CO}_2$  and implying  
103 reduced assimilation costs<sup>19</sup>. These two effects combine to yield a reduction of logit ( $\chi_o$ ) by  $\sim 0.0815$   
104 per km elevation ( $z$ ). The theoretical model for  $\chi_o$  can therefore be written in a linearized form:

$$105 \quad \ln [\chi_o / (1 - \chi_o)] \approx 0.0545 (T_g - 25) - 0.5 \ln D_0 - 0.0815 z + C \quad (1)$$

106 These predicted effects of each variable are shown here to be quantitatively consistent with the  
107 corresponding partial effects (that is, effects of each variable with the others held constant)  
108 independently inferred from the leaf  $\chi$  data by multiple regression (Fig. 1, Table 1). Fitting this  
109 equation (with fixed coefficients) to the data provided an estimate of  $C = 1.189$ , close to the value of

110 1.168 obtained with variable coefficients (Table 1). This constant is directly related to  $\beta$ , the ratio of  
111 carboxylation to transpiration cost factors at 25°C, by equation (12) in Methods. The coefficients in  
112 equation (1) were computed for standard conditions ( $T_g = 25$  °C,  $D_0 = 1$  kPa,  $z = 0$  km). The coefficient  
113 for elevation is sensitive to relative humidity (RH) at standard pressure, however, and becomes  
114 arbitrarily large as RH approaches 100%. The value of  $-0.0815$  was computed at RH = 50%. As  
115 predicted, the fitted (negative) slope of  $\ln [\chi / (1 - \chi)]$  with elevation increases with RH, most steeply at  
116 high RH (Fig. 1).

117  $\chi_o$  values from equation (1) are consistent with observed  $\chi$  across biomes ( $r = 0.51$ ) (Fig. 2).  
118 Highest values are in hot, wet, low-elevation sites (tropical forests), lowest in cold and/or dry and/or  
119 high-elevation sites (deserts, polar and alpine vegetation).  $\chi_o$  ranges globally from 0.4 to almost 1.0  
120 with a typical value of 0.77 (Supplementary Figure 2). The reduction from the equator towards mid-  
121 latitudes is due to increasing aridity while that in high latitudes is due to declining temperatures  
122 (Supplementary Figure 3).

123 Using a published dataset of CO<sub>2</sub> and water exchange measurements<sup>20</sup>, we confirmed  
124 (Supplementary Table 1) that the partial effects of temperature and vpd on instantaneous gas exchange  
125 are also consistent with equation (1). No elevation effect was found, however, probably due to the  
126 limited elevation range in this dataset.

127 So far, we have implicitly assumed infinite mesophyll conductance and, therefore, that the  
128 ratio ( $\chi_c$ ) of CO<sub>2</sub> partial pressure at the chloroplasts ( $c_c$ ) to  $c_a$  equals the ratio of  $c_i$  to  $c_a$ . In Methods we  
129 show that the optimal value of  $\chi_c$  has the same environmental dependencies as  $\chi_o$ , with an additional  
130 dependency on the ratio of  $g_s$  to  $g_m$ . Values of  $\chi_c$  were estimated from the leaf data using a process-  
131 based model for <sup>13</sup>C discrimination. Data analysis confirmed the predicted environmental responses of  
132 logit ( $\chi_c$ ), but with a lower estimate of  $C = 1.097$  (Supplementary Table 2) as expected, since finite  $g_m$   
133 implies  $\chi_c < \chi$ . The agreement between observed and predicted  $\chi_c$  was slightly improved compared to  
134 that of  $\chi$  (Supplementary Table 2, Supplementary Figure 4).

135 The co-ordination or co-limitation hypothesis, stating that the two photosynthetic processes of  
136 carboxylation and transport are coupled such that photosynthetic rates limited by those two processes  
137 are equal under typical daytime conditions, provides the next step towards a universal model of  
138 GPP<sup>21,22</sup>. The hypothesis implies adjustment of  $V_{cmax}$  in time and space to match environmental  
139 conditions<sup>22</sup> and predicts environmental responses of GPP in the field that are necessarily different  
140 from those observed in laboratory experiments which are typically conducted at light saturation, with  
141 no time for acclimation. Extensive field measurements also point to an optimal maximum rate of  
142 electron transport,  $J_{max}$ , that maximizes the photosynthetic benefits minus the costs of maintaining the  
143 electron-transport chain (Supplementary Figure 5)<sup>23</sup>. We can thereby eliminate both  $V_{cmax}$  and  $J_{max}$  as  
144 independent predictors, to derive a first-principles model for C<sub>3</sub> photosynthesis on weekly or longer  
145 time scales that has the mathematical form of a LUE model, but is nonetheless consistent with the  
146 standard model of C<sub>3</sub> photosynthesis:

147 
$$\text{GPP} = \varphi_0 I_{abs} m \sqrt{[1 - (c^*/m)^{2/3}]}$$
 (2)

148 where

149 
$$m = (c_a - \Gamma^*) / \{c_a + 2\Gamma^* + 3\Gamma^* \sqrt{[1.6 \eta^* D_0 \beta^{-1} (K + \Gamma^*)^{-1}]}\}$$
 (3)

150 Here  $\varphi_0$  is the intrinsic quantum yield ( $1.02 \text{ g C mol}^{-1}$ )<sup>24</sup>,  $I_{abs}$  is the absorbed photosynthetic  
 151 photon flux density (PPFD,  $\text{mol m}^{-2} \text{ s}^{-1}$ ),  $\Gamma^*$  is the photorespiratory compensation point (Pa),  $K$  is the  
 152 effective Michaelis-Menten coefficient of Rubisco (Pa),  $\eta^*$  is the viscosity of water relative to its value  
 153 at 25°C,  $\beta \approx 240$  from the constant  $C$  in equation (1), and  $c^*$  is proportional to the unit carbon cost for  
 154 the maintenance of electron transport capacity,  $\approx 0.41$  (estimated from observed  $J_{max}:V_{cmax}$  ratios).  
 155 Although not explored here, GPP of  $C_4$  plants under field conditions can be represented using a  
 156 modification of equations (2) and (3), given that  $C_4$  plants boost  $\text{CO}_2$  around the chloroplasts to high  
 157 levels while operating at a lower  $\varphi_0$ .

158 For  $C_3$  plants, the LUE is the product of  $\varphi_0$ ,  $m$  and the square-root term in equation (2). Thus  
 159 GPP is proportional to  $I_{abs}$ , which can be calculated as the product of incident PPFD and remotely  
 160 sensed green vegetation cover. LUE is less than the potential maximum ( $\varphi_0$ ) due to limitations by  $\text{CO}_2$   
 161 ( $m$ ) and electron transport capacity (the square-root term) leading to global mean reductions by 25%  
 162 and 43%, respectively. Supplementary Figure 6 shows how the predicted global pattern of potential  
 163 maximum GPP by  $C_3$  plants is modified by those constraints.

164 Predicted monthly GPP compares well with monthly GPP derived from  $\text{CO}_2$  flux  
 165 measurements (Fig. 3). Predicted global total annual GPP is 120 Pg C, within the accepted range<sup>25</sup>. The  
 166 model captures the variation in observed GPP within and among different biomes as well as or better  
 167 than other LUE models<sup>26</sup> (Supplementary Information, Supplementary Table 3). This level of  
 168 predictability, achieved with only two free parameters ( $\beta$  and  $c^*$ ) that are estimated from independent  
 169 observations, suggests that variations in  $\chi$  and LUE that are commonly represented by biome-specific  
 170 parameters could be explained more parsimoniously as a consequence of optimal plant responses to the  
 171 climates in which different biomes occur.

172 Enhanced LUE and GPP are predicted with increasing  $c_a$ , the magnitude of the enhancement  
 173 varying with climate. A meta-analysis of 12 Free Air Carbon dioxide Enrichment experiments showed  
 174 that with  $\text{CO}_2$  increased by about 200 ppm, LUE and instantaneous water use efficiency increased by  
 175  $12.2 \pm 9\%$  and  $54.3 \pm 17\%$ , while the ratio  $V_{cmax}/J_{max}$  and stomatal conductance changed by  $-4.9 \pm$   
 176  $2.8\%$  and  $-20 \pm 3\%$ <sup>27</sup>. The model-predicted mean changes in these quantities in turn (Supplementary  
 177 Information) are 17.2%, 55%, -22.4% and -15%. This analysis also showed a slight (non-significant)  
 178  $\text{CO}_2$ -induced reduction in  $\chi$ , consistent with the prediction of a slight decline by equation (9).  
 179 Considering finite  $g_m$  slightly enhances the LUE increase and reduces  $V_{cmax}/J_{max}$  decrease due to  $\text{CO}_2$   
 180 enrichment but has no effect on the responses of water use efficiency and  $g_s$ . The model's  
 181 overestimation of the  $\text{CO}_2$  effect on  $V_{cmax}/J_{max}$  requires further analysis: for example we note that  
 182 increased leaf temperature due to stomatal closure under  $\text{CO}_2$  enrichment would impose a strong  
 183 positive effect on  $V_{cmax}/J_{max}$  ( $\sim 4\%$  per K), potentially compensating the  $\text{CO}_2$  effect.

184 Consideration of finite  $g_m$  (substituting  $\chi_c$  for  $\chi_o$ ) affects the interpretation of  $\beta$ , which is  
185 reduced to  $\approx 200$  and now incorporates both the ratio of cost factors and the ratio of  $g_s$  to  $g_m$ . This  
186 modification reduces global annual GPP by 2.5% and marginally improves the agreement with  
187 observations ( $r = 0.742$ ,  $RMSE = 68.69 \text{ g C month}^{-1}$ ).

188 The spread of  $\chi$  and GPP values around the model predictions may reflect variation in  $\beta$  and  $c^*$   
189 which have so far been assumed constant. It will be worthwhile to explore their possible dependencies  
190 on plant functional traits. For example, the unit cost of transpiration is expected to depend on plant  
191 hydraulic traits, including the density and permeability of conducting tissue, plant height and the  
192 isohydry-anisohydry continuum, which together with soil moisture determines the maximum water  
193 potential difference between soil and leaf<sup>5</sup>. We found no significant difference in  $\chi$  between woody and  
194 non-woody plants; the differences in  $^{13}\text{C}$  discrimination among conventionally defined plant functional  
195 types (PFTs) were predicted correctly by climate and elevation alone (Supplementary Figure 7).  
196 Nonetheless, we did find a significant difference between gymnosperms and angiosperms (20% higher  
197 water cost in gymnosperms suggested by the global carbon isotope dataset: Supplementary  
198 Information) which could be explained by the narrower conducting elements of gymnosperms, and is  
199 consistent with the observed high intrinsic water use efficiency of conifer forests<sup>28</sup>. The unit cost of  
200  $V_{cmax}$  may be influenced by the costs of nitrogen uptake, which are likely higher (favouring investment  
201 in water transport) on less fertile soils. We tested for and detected a significant negative response of  $\chi$   
202 to soil pH, which indexes one dimension of soil fertility<sup>29</sup>, accounting for an additional 5% of variance  
203 in  $\chi$ . Predicted responses of the ratio  $J_{max}/V_{cmax}$  to temperature and  $\text{CO}_2$  made with the simplifying  
204 assumption of a universally constant  $c^*$  appear to be supported by observational evidence, but should be  
205 analysed with a more extensive dataset.

206 This simple model's predictive skill suggests a route towards an improved predictive  
207 understanding and modelling approach for terrestrial carbon and water cycling while providing a new  
208 theoretical framework for the analysis of both environmental and plant morphological influences on  
209 photosynthetic traits. By making testable predictions of such influences based on quantifiable benefits  
210 and costs, the evolutionary optimality approach may lead to a more robust basis for understanding and  
211 modelling both the co-ordination of plant traits among species, and biological controls of the emergent  
212 functional properties of ecosystems as represented in ESMs.

213 **Full Methods** and any associated references are available in the online version of the paper.

214 **Author Information** Correspondence and requests for materials should be addressed to H.W. and C.P.  
215 (wanghan\_sci@yahoo.com, peng.changhui@uqam.ca)

## 216 **Acknowledgements**

217 We thank Yan-Shih Lin, Vincent Maire, Belinda Medlyn, Beni Stocker, and IIASA colleagues for  
218 discussions, and Ralph Keeling for comments on successive drafts. The paper is a contribution to the  
219 AXA Chair Programme on Biosphere and Climate Impacts and Imperial College's initiative on Grand  
220 Challenges in Ecosystems and the Environment. Research is supported by National Basic Research

221 Programme of China (2013CB956602) grant to CP and HW, National Natural Science Foundation of  
222 China (Grant no. 31600388) to HW, an Australian Research Council Discovery grant ('Next-  
223 generation vegetation model based on functional traits') to ICP and IJW, an Australian National Data  
224 Service (ANDS) grant ('Ecosystem production in space and time') to ICP, and Terrestrial Ecosystem  
225 Research Council (TERN) grants ('Ecosystem Modelling and Scaling Infrastructure') to ICP and BJE.  
226 TERN and ANDS are supported by the Australian Government National Collaborative Infrastructure  
227 Strategy (NCRIS). TFK acknowledges financial support from the Laboratory Directed Research and  
228 Development (LDRD) fund under the auspices of DOE, BER Office of Science at Lawrence Berkeley  
229 National Laboratory, and a Macquarie University Research Fellowship. In addition to authors of this  
230 paper, data were provided by Margaret Barbour, Lucas Cernusak, Todd Dawson, David Ellsworth,  
231 Graham Farquhar, Howard Griffiths, Claudia Keitel, Alexander Knohl, Peter Reich, Dave Williams,  
232 Radika Bhaskar, Hans Cornelissen, Anna Richards, Susanne Schmidt, Fernando Valladares, Christian  
233 Körner, Ernst-Detlef Schulze, Nina Buchmann and Lou Santiago. We used 'free and fair use' eddy-  
234 covariance data acquired by the FLUXNET community and, in particular, by the following networks:  
235 AmeriFlux (US Department of Energy, Biological and Environmental Research, Terrestrial Carbon  
236 Program), AsiaFlux, CarboEuropeIP, Fluxnet-Canada (supported by CFCAS, NSERC, BIOCAP,  
237 Environment Canada, and NRCan), OzFlux and TCOS-Siberia. We acknowledge the financial support  
238 to the eddy-covariance data harmonization provided by CarboEuropeIP, FAO- GTOS-TCO, iLEAPS,  
239 Max Planck Institute for Biogeochemistry, National Science Foundation, University of Tuscia,  
240 Université Laval and Environment Canada and US Department of Energy and the database  
241 development and technical support from Berkeley Water Center, Lawrence Berkeley National  
242 Laboratory, Microsoft Research eScience, Oak Ridge National Laboratory, University of California-  
243 Berkeley, University of Virginia.

#### 244 **Author contributions**

245 H.W. and I.C.P. derived the predictions. H.W. carried out all the analyses and constructed the Figures  
246 and Tables. I.C.P. and T.F.K. contributed to the analysis and writing. T.W.D., B.J.E. and I.C.P.  
247 developed and tested the flux partitioning method. T.W.D. developed the global flux database and all  
248 the GPP computations. I.J.W. proposed least-cost hypothesis and contributed to the analysis. W.K.C.  
249 originated and compiled the  $\Delta^{13}\text{C}$  data set. H.W. and I.C.P. wrote the first draft, and all authors  
250 contributed to the final draft.

251 **Competing financial interests** The authors declare no competing financial interests.

#### 252 **References**

- 253 1 Ciais, P. *et al.* Carbon and other biogeochemical cycles. in *Climate change 2013: the physical*  
254 *science basis. Contribution of Working Group I to the Fifth Assessment Report of the*  
255 *Intergovernmental Panel on Climate Change* (eds Thomas F Stocker *et al.*) Ch. 6, 465-570  
256 (Cambridge University Press, 2014).
- 257 2 Friedlingstein, P. *et al.* Uncertainties in CMIP5 climate projections due to carbon cycle  
258 feedbacks. *Journal of Climate* **27**, 511-526 (2014).



259 3 Prentice, I. C., Liang, X., Medlyn, B. E. & Wang, Y. P. Reliable, robust and realistic: the three  
260 R's of next-generation land-surface modelling. *Atmospheric Chemistry and Physics* **15**, 5987-  
261 6005 (2015).

262 4 Wang, H., Prentice, I. C. & Davis, T. W. Biophysical constraints on gross primary production  
263 by the terrestrial biosphere. *Biogeosciences* **11**, 5987-6001 (2014).

264 5 Prentice, I. C., Dong, N., Gleason, S. M., Maire, V. & Wright, I. J. Balancing the costs of  
265 carbon gain and water transport: testing a new theoretical framework for plant functional  
266 ecology. *Ecology letters* **17**, 82-91 (2014).

267 6 Wright, I. J., Reich, P. B. & Westoby, M. Least - Cost Input Mixtures of Water and Nitrogen  
268 for Photosynthesis. *The American Naturalist* **161**, 98-111 (2003).

269 7 Monteith, J. L. Solar radiation and productivity in tropical ecosystems. *Journal of Applied*  
270 *Ecology* **9**, 747-766 (1972).

271 8 Farquhar, G. D., von Caemmerer, S. & Berry, J. A. A biochemical model of photosynthetic  
272 CO<sub>2</sub> assimilation in leaves of C<sub>3</sub> species. *Planta* **149**, 78-90 (1980).

273 9 Medlyn, B. E. Physiological basis of the light use efficiency model. *Tree Physiology* **18**, 167-  
274 176 (1998).

275 10 Ali, A. *et al.* A global scale mechanistic model of the photosynthetic capacity. *Geoscientific*  
276 *Model Development Discussions* **8**, 6217–6266 (2015).

277 11 Cai, W. *et al.* Large differences in terrestrial vegetation production derived from satellite-  
278 based light use efficiency models. *Remote Sensing* **6**, 8945-8965 (2014).

279 12 De Kauwe, M. G. *et al.* Forest water use and water use efficiency at elevated CO<sub>2</sub>: a model -  
280 data intercomparison at two contrasting temperate forest FACE sites. *Global Change Biology*  
281 **19**, 1759-1779 (2013).

282 13 Medlyn, B. E. *et al.* Reconciling the optimal and empirical approaches to modelling stomatal  
283 conductance. *Global Change Biology* **17**, 2134-2144 (2011).

284 14 Diefendorf, A. F., Mueller, K. E., Wing, S. L., Koch, P. L. & Freeman, K. H. Global patterns  
285 in leaf  $\delta^{13}\text{C}$  discrimination and implications for studies of past and future climate. *Proceedings*  
286 *of the National Academy of Sciences* **107**, 5738-5743 (2010).

287 15 Cowan, I. & Farquhar, G. Stomatal function in relation to leaf metabolism and environment.  
288 *Symposia of the Society for Experimental Biology*, 471-505 (1977).

289 16 Givnish, T. J. *On the Economy of Plant Form and Function*. Vol. 6 (Cambridge University  
290 Press, 1986).

291 17 Cornwell, W. K. *et al.* A global dataset of leaf  $\Delta^{13}\text{C}$  values. doi:10.5281/zenodo.569501  
292 (2017).

293 18 Farquhar, G. D., Ehleringer, J. R. & Hubick, K. T. Carbon isotope discrimination and  
294 photosynthesis. *Annual review of plant biology* **40**, 503-537 (1989).

295 19 Körner, C., Farquhar, G. & Wong, S. Carbon isotope discrimination by plants follows  
296 latitudinal and altitudinal trends. *Oecologia* **88**, 30-40 (1991).

297 20 Lin, Y.-S. *et al.* Optimal stomatal behaviour around the world. *Nature Climate Change* **5**,  
298 459–464 (2015).

299 21 Maire, V. *et al.* The coordination of leaf photosynthesis links C and N fluxes in C3 plant  
300 species. *PloS one* **7**, e38345 (2012).

301 22 Haxeltine, A. & Prentice, I. C. A general model for the light-use efficiency of primary  
302 production. *Funct. Ecol.* **10**, 551-561, doi:10.2307/2390165 (1996).

303 23 Kattge, J. & Knorr, W. Temperature acclimation in a biochemical model of photosynthesis: a  
304 reanalysis of data from 36 species. *Plant, cell & environment* **30**, 1176-1190 (2007).

305 24 Collatz, G., Berry, J., Farquhar, G. & Pierce, J. The relationship between the Rubisco reaction  
306 mechanism and models of photosynthesis. *Plant, Cell & Environment* **13**, 219-225 (1990).

307 25 Beer, C. *et al.* Terrestrial gross carbon dioxide uptake: global distribution and covariation with  
308 climate. *Science* **329**, 834-838 (2010).

309 26 Yuan, W. *et al.* Global comparison of light use efficiency models for simulating terrestrial  
310 vegetation gross primary production based on the LaThuile database. *Agricultural and forest  
311 meteorology* **192**, 108-120 (2014).

312 27 Ainsworth, E. A. & Long, S. P. What have we learned from 15 years of free - air CO<sub>2</sub>  
313 enrichment (FACE)? A meta - analytic review of the responses of photosynthesis, canopy  
314 properties and plant production to rising CO<sub>2</sub>. *New Phytologist* **165**, 351-372 (2005).

315 28 Frank, D. C. *et al.* Water-use efficiency and transpiration across European forests during the  
316 Anthropocene. *Nature Climate Change* **5**, 579-583 (2015).

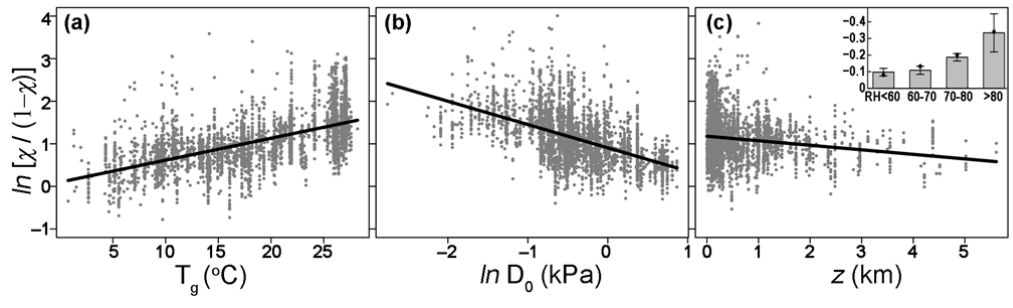
317 29 Maire, V. *et al.* Global effects of soil and climate on leaf photosynthetic traits and rates.  
318 *Global Ecology and Biogeography* **24**, 706-717 (2015).

319 30 Kaplan, J. O. Geophysical applications of vegetation modeling. (Lund University, 2001).

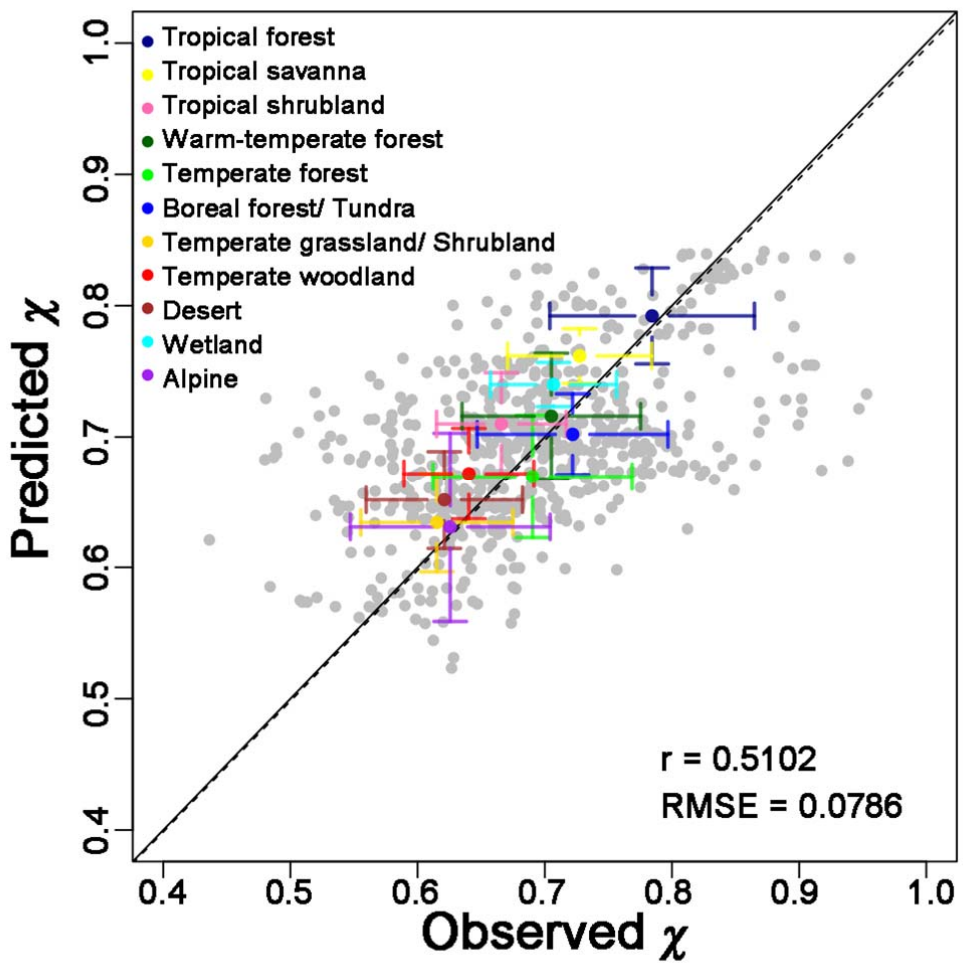
320 **Table 1 | Summary statistics for the environmental dependencies of  $\chi$  (the ratio of leaf-internal to**  
321 **ambient CO<sub>2</sub> partial pressure).** Logit-transformed values of  $\chi$  derived from the global leaf stable  
322 carbon isotope dataset using a standard method<sup>18</sup> were regressed against the difference between  
323 growing-season mean temperature  $T_g$  and 25°C ( $\Delta T_g$ , °C), the natural logarithm of growing-season  
324 mean vapour pressure deficit at standard atmospheric pressure ( $\ln D_0$ , kPa), and elevation ( $z$ , km).  
325 Theoretical values, shown for comparison, are partial derivatives of logit-transformed predicted  
326 ‘optimal’  $\chi$  with respect to each predictor, evaluated for standard conditions ( $T_g = 25$  °C,  $D_0 = 1$  kPa,  $z$   
327 = 0 km).  
328

Predictor	Theoretical value	Fitted coefficient	Confidence intervals		Multiple R <sup>2</sup>
			2.5%	97.5%	
$\Delta T_g$	<b>0.0545</b>	0.0515	0.0456	0.0575	0.391
$\ln D_0$	<b>-0.5</b>	-0.5478	-0.6111	-0.4846	
$z$	<b>-0.0815</b>	-0.1065	-0.1315	-0.0815	
intercept	<b>1.189</b>	1.1680	1.0464	1.2896	

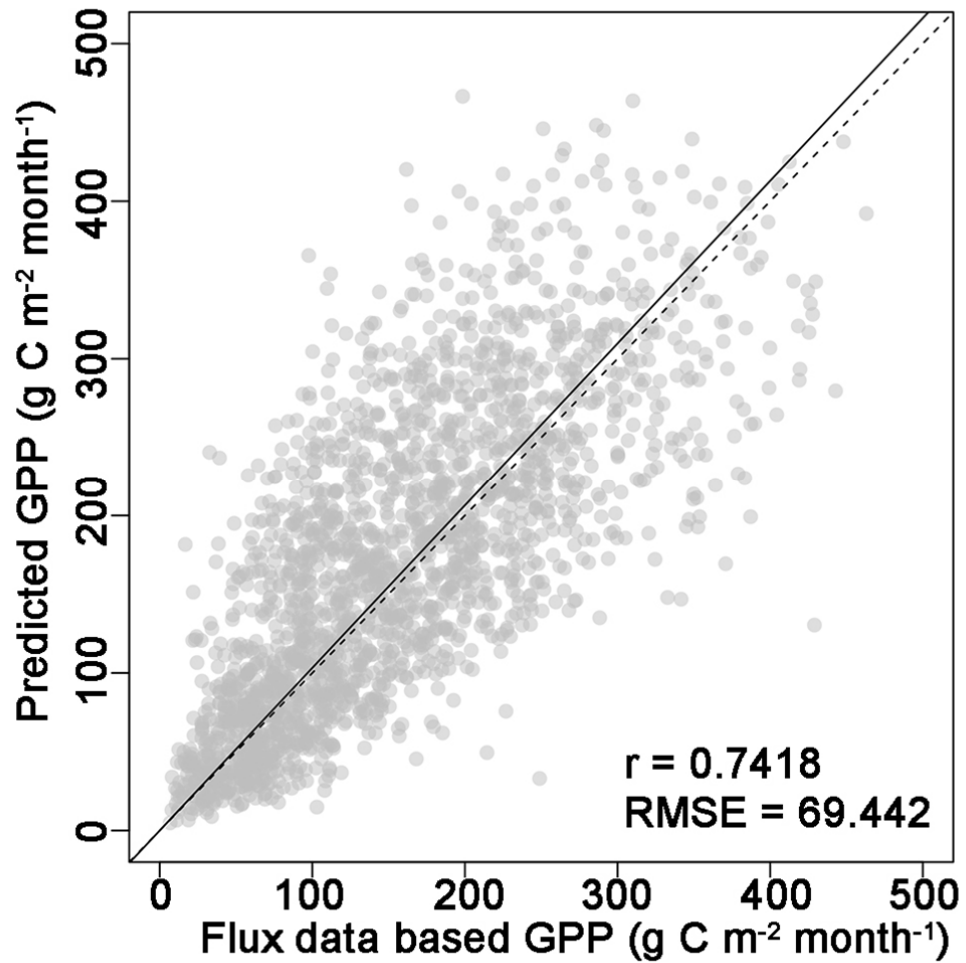
329 **Figure 1 | Partial residual plots from the regression of logit-transformed values of  $\chi$  (the ratio of**  
330 **leaf-internal to ambient CO<sub>2</sub> partial pressure) derived from the global leaf stable carbon isotope**  
331 **dataset against environmental predictors.  $T_g$ : growing-season mean temperature.  $\ln D_0$ : the natural**  
332 **logarithm of growing-season mean vapour pressure deficit at standard atmospheric pressure.  $z$ :**  
333 **elevation. Inset shows elevation responses for relative humidity (RH, %) classes with error bars**  
334 **showing 95% confidence intervals, compared to predicted responses (black dots) evaluated at the**  
335 **centre of each RH class.**



336 **Figure 2 | Site-mean values of the ratio of leaf-internal to ambient CO<sub>2</sub> partial pressure ( $\chi$ ).**  
 337 Predictions ( $\chi_o$ ) are from the theoretical model driven by three environmental predictors (equation 1).  
 338 Observations ( $\chi$ ) are from the global leaf stable carbon isotope dataset. Mean and standard deviation  
 339 are shown for each biome. Biome types were assigned based on BIOME4<sup>30</sup> for consistency except for  
 340 ‘wetland’ and ‘alpine’ types, which were assigned from source publications. The solid line is the  
 341 regression through the origin; the dashed line is the 1:1 line.  $r$ : Pearson correlation between observed  
 342 and predicted values; RMSE: root-mean-squared error of prediction.



343 **Figure 3 | Monthly gross primary production (GPP) at flux sites.** Predictions from equations (2)  
344 and (3); observations based on CO<sub>2</sub> flux data in the FLUXNET archive. The solid line is the regression  
345 through the origin; the dashed line is the 1:1 line. *r*: Pearson correlation between observed and  
346 predicted values; RMSE: root-mean-squared error of prediction.



347 **Methods**

348 **Theory for the environmental controls on  $\chi$**

349 Optimality hypotheses to account for the environmental responses of stomata have a long history, with  
350 pioneering contributions especially by Cowan and Farquhar and Givnish<sup>15,16</sup>. Cowan and Farquhar  
351 hypothesized that stomata act to maximize marginal carbon gain (assimilation,  $A$ ) while minimizing  
352 marginal water loss (transpiration,  $E$ ), i.e.  $\partial E / \partial A = \lambda$  where  $\lambda$  is a parameter representing the ‘marginal  
353 carbon cost of water’. This approach successfully addresses many observed features of stomatal  
354 behaviour but leaves the value of  $\lambda$  undefined and, as noted by Givnish, does not explicitly consider the  
355 costs of maintaining photosynthetic capacity. These limitations are avoided by the *least-cost*  
356 *hypothesis*, which states that plants should minimize the combined carbon costs (per unit of  
357 assimilation) of maintaining the required capacities for carboxylation and transpiration. This hypothesis  
358 was first proposed explicitly by Wright et al.<sup>6</sup>, and applied in the context of the standard model of  
359 photosynthesis<sup>8</sup> by Prentice et al.<sup>5</sup> who defined the following optimality criterion for  $\chi$ :

360 
$$a \cdot \partial(E/A) / \partial \chi + b \cdot \partial(V_{cmax}/A) / \partial \chi = 0 \quad (4)$$

361 Here,  $a$  and  $b$  are dimensionless cost factors for  $E$  and  $V_{cmax}$  respectively.

362 The *coordination hypothesis* states that  $V_{cmax}$  of leaves at any level in the canopy acclimates spatially  
363 and temporally to the prevailing daytime incident PPFD (the absorbed photosynthetic photon flux  
364 density) in such a way as to be neither in excess (entailing additional, futile maintenance respiration),  
365 nor less than required for full exploitation of the available light<sup>21,22,31</sup>. In other words, under typical  
366 daytime conditions when most photosynthesis takes place, the Rubisco-limited photosynthetic rate is  
367 equal to electron-transport limited photosynthetic rate ( $A=A_c=A_j$ ). Therefore, Rubisco-limited  
368 photosynthesis in the standard biochemical model<sup>8</sup> can be rewritten as a prediction of  $V_{cmax}/A$ :

369 
$$V_{cmax}/A = (\chi c_a + K) / (\chi c_a - \Gamma^*), \quad (5)$$

370 Fick’s law of diffusion applied to both H<sub>2</sub>O and CO<sub>2</sub> allows prediction of  $E/A$ :

371 
$$E/A = 1.6(D/c_a)/(1-\chi) \quad (6)$$

372 where  $D$  is vapour pressure deficit. Initially neglecting  $\Gamma^*$  for simplicity (i.e. assuming  $\chi c_a \gg \Gamma^*$ ),  
373 substituting equations (5) and (6) in (4) and taking derivatives, the optimal value of  $\chi$  satisfies:

374 
$$1.6(aD/c_a)/(1-\chi)^2 - bK/\chi^2 c_a = 0 \quad (7)$$

375 The solution to equation (7) provides the required optimal value ( $\chi_o$ ):

376 
$$\chi_o = \zeta / (\zeta + \sqrt{D}), \text{ where } \zeta = \sqrt{(bK/1.6a)} \quad (8)$$

377 Omitting the assumption  $\chi c_a \gg \Gamma^*$  yields the more exact form:

378  $\chi_o = \Gamma^*/c_a + (1 - \Gamma^*/c_a) \zeta/(\zeta + \sqrt{D})$ , where  $\zeta = \sqrt{[b(K + \Gamma^*)/1.6a]}$  (9)

379 The parameter  $\zeta$  expresses the sensitivity of  $\chi_o$  to  $D$ . The ratio of stem respiration to transpiration  
 380 capacity ( $a$ ) depends (among other things) on the viscosity of water. The ratio of mitochondrial  
 381 respiration to carboxylation capacity ( $b$ ) is generally taken as constant<sup>8</sup>. As only the ratio  $b/a$  (not the  
 382 individual terms  $b$  and  $a$ ) affects  $\chi_o$ , we will later use the composite parameter  $\beta$  to denote the value of  
 383  $b/a$  at 25°C.

384 Given the particular form of equation (8), logit transformation simplifies the derivation of its  
 385 sensitivities to environmental variables, as follows:

386  $\text{logit}(\chi_o) = \ln[\chi_o/(1 - \chi_o)] = \frac{1}{2} \ln b - \frac{1}{2} \ln a + \frac{1}{2} \ln K - \frac{1}{2} \ln D - \frac{1}{2} \ln 1.6$  (10)

387 The dependencies of  $a$  (through the viscosity of water  $\eta$ ) and  $K$  (through the Michaelis-Menten  
 388 coefficients of Rubisco for carboxylation ( $K_c$ ) and oxygenation ( $K_o$ )) on temperature ( $T$ ), and the  
 389 dependency of  $K$  (through  $P_o$ , the partial pressure of O<sub>2</sub>) and  $D$  on elevation, are denoted by  $f_1(T)$ ,  $f_2(T)$ ,  
 390  $g_1(z)$  and  $g_2(z)$ . The elevation effect here includes the effect of the vapour pressure decline because  
 391 humidity statistics in the 3D-gridded datasets used for global analysis do not account for it. Thus, we  
 392 substitute  $D$  with  $D_0$  (the vpd that would be obtained at standard atmospheric pressure under the same  
 393 temperature and H<sub>2</sub>O mole fraction). Equation (10) is then equivalent to:

394  $\ln[\chi_o/(1 - \chi_o)] = -\frac{1}{2} \ln f_1(T) + \frac{1}{2} \ln f_2(T) + \frac{1}{2} \ln g_1(z) - \frac{1}{2} \ln D_0 - \frac{1}{2} \ln g_2(z) + C$ , (11)

395 where  $C = \frac{1}{2} (\ln b - \ln a_{ref} + \ln K_{ref} - \ln 1.6) = \frac{1}{2} (\ln \beta + \ln K_{ref} - \ln 1.6)$  (12)

396  $a_{ref}$  and  $K_{ref}$  are the values of  $a$  and  $K$  under standard conditions ( $T = 298$  K,  $z = 0$ ). Equation (11)  
 397 predicts the coefficient of  $\ln D_0$  as  $-0.5$ .

### 398 **Temperature dependency of $a$**

399 The parameter  $a$  is directly proportional to  $\eta$ , according to equation (11) in ref. 5. The temperature  
 400 dependency of  $\eta$  can be well approximated by the Vogel equation<sup>32</sup>:

401  $\eta = 10^{-3} \exp [A + B/(C + T)]$  (13)

402 where  $A = -3.719$ ,  $B = 580$  and  $C = -138$ . Thus, the sensitivity of  $\eta$  to temperature is given by:

403  $(1/\eta) \partial \eta / \partial T = \partial \ln \eta / \partial T = -B/(C + T)^2$  (14)

404 allowing the response of  $\eta$  to  $T$ , within the physiologically relevant range, to be well approximated by  
 405 an exponential response to  $\Delta T = T - 298$  K relative to a reference value at  $T = 298$  K ( $\eta_{ref}$ ):

406  $f_1(T) = \eta/\eta_{ref} \approx \exp [-B/(C + T)^2 \Delta T]$  (15)



407 **Temperature and elevation dependencies of  $K$**

408  $K$  (in partial pressure units) is given by:

409 
$$K = K_c (1 + P_o/K_o), \quad (16)$$

410  $P_o$  can be expressed as a simple function of elevation (in km) using a standard approximation for the  
411 decline in atmospheric pressure with elevation<sup>33</sup>:

412 
$$P_o = 21000 \exp(-0.114 z) \quad (17)$$

413 The Arrhenius relationship describing the response of a biochemical rate parameter ( $x$ , such as  $K_c$  and  
414  $K_o$ ) to temperature can be expressed as:

415 
$$\partial \ln x / \partial T = (\Delta H/R) \cdot (1/T^2) \quad (18)$$

416 where  $R = 8.3145 \text{ J mol}^{-1} \text{ K}^{-1}$  and the activation energies  $\Delta H$  are  $79.43 \text{ kJ mol}^{-1}$  for  $K_c$  and  $36.38 \text{ kJ}$   
417  $\text{mol}^{-1}$  for  $K_o$ , denoted as  $\Delta H_c$  and  $\Delta H_o$ , respectively, from *in vivo* determinations<sup>34</sup>.

418 Therefore, the sensitivity of  $K$  to temperature from equation (16) is given by:

419 
$$(1/K) \partial K / \partial T = [(\Delta H_c/R)(1/T^2) (P_o + K_o) - (\Delta H_o/R)(1/T^2) P_o] / (P_o + K_o) \quad (19)$$

420 leading to:

421 
$$f_2(T) = \exp([( \Delta H_c/R)(1/T^2) (P_o + K_o) - (\Delta H_o/R)(1/T^2) P_o] / (P_o + K_o) \Delta T) \quad (20)$$

422 The sensitivity of  $K$  to elevation due to declination in  $P_o$  can then be derived from equation (16):

423 
$$(1/K) \partial K / \partial z = -0.114 P_o / (P_o + K_o) \quad (21)$$

424 Therefore,

425 
$$g_1(z) = \exp[-0.114 P_o / (P_o + K_o) z] \quad (22)$$

426 **Elevation dependency of  $D$**

427  $D$  can similarly be expressed as a function of elevation:

428 
$$D = e_s - e_{a0} \exp(-0.114 z) \quad (23)$$

429 where  $e_s$  is the saturation vapour pressure and  $e_{a0}$  is the actual vapour pressure that would be obtained  
430 at sea level under the same  $\text{H}_2\text{O}$  mole fraction and temperature. Since  $\exp(-0.114z)$  can be taken as  
431 equal to unity, to a good approximation, within the relevant range of  $z$ , the dependency of  $D$  on  
432 elevation here approximated as:

433  $\partial \ln D / \partial z = 0.114 e_{a0} / D_0 = 0.114 RH / (1 - RH),$  (24)

434 Therefore,

435  $g_2(z) = \exp \{0.114 [RH / (1 - RH)] z\}$  (25)

436 Note that this theoretically derived elevation effect on  $D$  varies strongly with  $RH$ , approaching infinity  
437 as  $RH$  tends to 1.

438 ***Linearized expressions for  $\chi_o$  in terms of environmental predictors***

439 Evaluating equations (15), (20), (22) and (25) at standard temperature ( $T = 298$  K,  $z = 0$  and  $RH_0 =$   
440 50%) and substituting the resulting expressions in equation (11), we obtain:

441  $\ln [\chi_o / (1 - \chi_o)] = \frac{1}{2} (0.0864 + 0.0227) \Delta T - \frac{1}{2} (0.0491 + 0.114) z - \frac{1}{2} \ln D_0 + C$   
442  $= 0.0545 \Delta T - 0.0815 z - 0.5 \ln D_0 + C$  (26)

443  $C \approx 1.189$ , estimated as the intercept in a generalized linear model (GLM) fitted to the data with  
444 imposed regression coefficients for all three environmental effects in equation (26). This allows us to  
445 estimate  $\beta \approx 240$  from equation (12). Therefore, the optimal leaf-internal partial pressure of  $\text{CO}_2$  can be  
446 derived from the more exact expression for  $\chi_o$  (equation 9):

447  $c_i = \frac{\xi c_a + \Gamma^* \sqrt{D}}{\xi + \sqrt{D}}, \xi = \sqrt{\frac{\beta(K + \Gamma^*)}{1.6\eta^*}}$ , (27)

448 Here  $\eta^*$  is the viscosity of water relative to its value at 25°C, representing the effect of changing  
449 viscosity on the value of  $a$ .

450 **Testing the theory with global  $\delta^{13}\text{C}$  data**

451 Vascular-plant leaf stable carbon isotope data were compiled from published and unpublished  
452 sources<sup>17</sup>. Inferred carbon isotope discrimination ( $\Delta$ ) values for 3549 leaf samples of  $\text{C}_3$  plants were  
453 converted to estimates of  $\chi$  by a standard equation<sup>18</sup>:

454  $\chi = \frac{\Delta - a'}{b' - a'}$  (28)

455 where  $a'$  and  $b'$  have standard values 4.4 and 27, representing the diffusional and biochemical  
456 components of carbon isotope discrimination, respectively. The Climatic Research Unit CL2.0 10-  
457 minute gridded monthly climatology<sup>35</sup> of mean, maximum and minimum temperatures and relative  
458 humidity provided mean temperature ( $T_g$ , °C) and vapour pressure deficit ( $D_0$ , kPa) values for the  
459 period with daily mean temperatures  $> 0^\circ\text{C}$ . Values of  $\ln [\chi / (1 - \chi)]$  were fitted using a GLM with  $\Delta T_g =$   
460  $T_g - 25^\circ\text{C}$ ,  $\ln D_0$ , and site-specific elevation ( $z$ , km) as predictors. Standard errors estimated by the

461 GLM were combined quadratically with standard errors for the uncertainty of the effective Rubisco  
 462 discrimination parameter  $b'$ , the latter obtained by generating  $10^4$  normally distributed values of  $b'$   
 463 (mean = 27, standard deviation = 0.27) and repeating the estimation of  $\chi$  and the GLM fitting  $10^4$  times  
 464 with different  $b'$  values.

465 **Incorporating finite  $g_m$  into the least-cost framework and testing with global  $\delta^{13}\text{C}$  data**

466 Mesophyll conductance, the liquid-phase conductance between the intercellular spaces and the  
 467 chloroplasts, is assumed arbitrarily large in most large-scale ecophysiological data analysis and  
 468 models<sup>36</sup>, since the mechanisms behind its environmental responses remain unclear. The prediction of  
 469  $g_m$  still largely relies on empirical relationships<sup>37</sup>. However, the effect of finite  $g_m$  can be incorporated  
 470 into the least-cost framework naturally due to its impact on carboxylation, and furthermore leads to an  
 471 optimal ratio of the chloroplastic to ambient  $\text{CO}_2$  ( $\chi_c$ ) under the simplifying assumption that the ratio of  
 472  $g_s$  (stomata conductance) to  $g_m$  is independent of environmental factors<sup>38-41</sup>.

473 Assuming that the total conductance ( $g$ ) for  $\text{CO}_2$  diffusing from the ambient atmosphere to the  
 474 chloroplasts is principally controlled by  $g_s$  and  $g_m$ :

$$475 \quad 1/g = 1/g_s + 1/g_m \quad (29)$$

476 Note that  $g_m$  affects  $\text{CO}_2$  diffusion for carboxylation, but not  $\text{H}_2\text{O}$  diffusion during transpiration.  
 477 Replacing stomatal with total conductance for carboxylation, equation (6) therefore becomes:

$$478 \quad E/A = 1.6 (D/c_a) (g_s + g_m) / [(1 - \chi_c) g_m] \quad (30)$$

479 The leaf-internal  $\text{CO}_2$  concentration ( $\chi_c c_a$ ) in equation (5) can then be replaced by the chloroplastic  $\text{CO}_2$   
 480 concentration ( $\chi_c c_a$ ):

$$481 \quad V_{cmax} / A = (\chi_c c_a + K) / (\chi_c c_a - \Gamma^*) \quad (31)$$

482 Applying the optimality criterion:

$$483 \quad a \cdot \partial(E/A_c) / \partial \chi_c + b \cdot \partial(V_{cmax} / A_c) / \partial \chi_c = 0 \quad (32)$$

484 to equations (30) and (31), the optimal ratio of chloroplast to ambient  $\text{CO}_2$  ( $\chi_{co}$ ) is given by (assuming  
 485  $\chi_c c_a \gg \Gamma^*$ ):

$$486 \quad \chi_{co} = \zeta_c / (\zeta_c + \sqrt{D}), \text{ where } \zeta_c = \sqrt{[bK/1.6a/(1 + g_s/g_m)]} = \zeta / \sqrt{(1 + g_s/g_m)}, \quad (33)$$

487 or, if we relax the assumption  $\chi_c c_a \gg \Gamma^*$ , by:

$$488 \quad \chi_{co} = \Gamma^* / c_a + (1 - \Gamma^* / c_a) \zeta_c / (\zeta_c + \sqrt{D}), \text{ where } \zeta_c = \sqrt{\{b(K + \Gamma^*) / [1.6a(1 + g_s/g_m)]\}} \quad (34)$$

489 Here  $\chi_{co}$  is not influenced by  $g_s$  and  $g_m$  separately, but by their ratio. The form of the model for  $\chi_{co}$   
 490 resembles that for  $\chi_o$ , but the sensitivity parameter  $\zeta$  is adjusted by a factor  $\sqrt{[1/(1 + g_s/g_m)]}$ .

491 In the model for  $\chi_{co}$  the ratio of  $g_s$  to  $g_m$  is assumed to be independent of environment. Even though  
 492 both  $g_s$  and  $g_m$  vary with environmental conditions, including light, moisture and temperature, their  
 493 covariation under a wide range of conditions supports this assumption at least as a first  
 494 approximation<sup>38-41</sup>. Moreover, data indicate that the value of  $g_s/g_m$  is quite conservative, with a median  
 495 of about 1.4 (I.J. Wright, unpublished data). The derivation of the environmental dependencies of  $\chi_{co}$   
 496 then follows the same logical steps as that for  $\chi$ . Further refinement of the model for  $\chi_{co}$  however would  
 497 require deeper understanding of the regulation of  $g_s$  and  $g_m$ .

498 The estimated value of the ratio of cost factors  $b$  to  $a$  at reference temperature is updated to a value of  
 499 343 after deducting the term of  $(g_s/g_m + 1)^{-1}$  from constant  $C$ . This time we obtained  $C$  based on  
 500 observational  $\chi_c$  estimated from the global carbon isotope dataset with the “comprehensive” equation in  
 501 Ubierna & Farquhar<sup>42</sup> but following the first three simplifying assumptions listed in their Figure 1: (1)  
 502 that the ternary effect is negligible; (2) the fractionations associated with Rubisco carboxylation, during  
 503 respiration and photorespiration are far less than 1; (3) infinite boundary-layer conductance. We also  
 504 assumed leaf dark respiration  $R_d \ll A$ , so that  $R_d/(R_d + A) \approx R_d/A$ . The “comprehensive” equation for  $\Delta$   
 505 can then be rewritten more simply as:

$$506 \quad \Delta = a_s (1 - \chi) + a_m (\chi - \chi_c) + b\chi_c - eb_0(\chi_c + \kappa) - f\gamma \quad (35)$$

507 Here,  $a_s$ ,  $a_m$ ,  $b$ ,  $e$  and  $f$  are the fractionations associated with diffusion in air (4.4‰), in water (1.8‰),  
 508 by Rubisco carboxylation (27 to 30‰), during respiration (0 to -5‰) and photorespiration (8 to 16‰),  
 509 respectively.  $b_0 = R_d/V_{cmax} = 0.015^8$ ,  $\kappa = K/c_a$  and  $\gamma = \Gamma^*/c_a$ .

510 Given that the CO<sub>2</sub> flux from the outside to the intercellular spaces must be the same as that from the  
 511 intercellular spaces to the chloroplast, denoting the ratio of  $g_m$  to  $g_s$  as  $\theta$ , we have:

$$512 \quad (1 - \chi) g_s = (\chi - \chi_c) \theta g_s \quad (36)$$

513 Therefore:

$$514 \quad 1 - \chi = \theta (1 - \chi_c)/(1 + \theta) \quad (37)$$

515 and

$$516 \quad \chi - \chi_c = (1 - \chi_c)/(1 + \theta) \quad (38)$$

517 Substituting these expressions into equation (35) and solving for  $\chi_c$  gives:

$$518 \quad \chi_c = \frac{\Delta - \frac{\theta a_s + a_m}{1 + \theta} + eb_0 \kappa + f\gamma}{b - \frac{\theta a_s + a_m}{1 + \theta} - eb_0} \quad (39)$$

519 We assumed a constant value of  $\theta = 1.4$ , based on data compiled by IJW, and consistent with values in  
 520 the literature<sup>43</sup>.

521 Given the uncertainties in parameters  $b$ ,  $e$  and  $f$ , we chose the values ( $b = 30$ ,  $e = 0$ ,  $f = 16$ ) that  
 522 produced the best fit ( $R^2 = 0.5057$ ) in the regression of  $\chi_c$  against temperature,  $\ln$  vpd and elevation  
 523 (Supplementary Table 2).

#### 524 **Light-use efficiency model**

525 The model proposed by Wang et al.<sup>4</sup> assumed that the electron-transport and Rubisco-limited rates of  
 526 photosynthesis ( $A_J$ ,  $A_c$ ) as described by the biochemical photosynthesis model<sup>8</sup> are coordinated (that is,  
 527  $A = A_J = A_c$ ) under typical daytime conditions<sup>21,22,31</sup>, allowing GPP to be predicted from  $A_J$  at a monthly  
 528 time scale by:

$$529 \quad A_J = \varphi_0 I_{abs} (c_i - \Gamma^*) / (c_i + 2\Gamma^*) \quad (40)$$

530 LUE is the product of  $\varphi_0$  and the CO<sub>2</sub> limitation term of  $(c_i - \Gamma^*) / (c_i + 2\Gamma^*)$  (denoted here by  $m$ ).  
 531 Incorporating the exact equation for  $c_i$  (equation 27) yields:

$$532 \quad A = \varphi_0 I_{abs} m \quad (41)$$

533 where

$$534 \quad m = \frac{c_a - \Gamma^*}{c_a + 2\Gamma^* + 3\Gamma^* \sqrt{\frac{1.6D\eta^*}{\beta(K + \Gamma^*)}}} \quad (42)$$

535 Equations (41) and (42) assume that the light response of  $A$  is linear up to the coordination point, i.e.  
 536 that the maximum electron-transport rate ( $J_{max}$ ) is arbitrarily large. In reality  $J_{max}$  limitation can be  
 537 significant, especially at high temperatures. We therefore modified equation (41) to allow for a non-  
 538 rectangular hyperbola relationship between  $A$  and  $I_{abs}$ <sup>44,45</sup>.

$$539 \quad A = \varphi_0 I_{abs} m \frac{1}{\sqrt{1 + \left( \frac{4\varphi_0 I_{abs}}{J_{max}} \right)^2}} \quad (43)$$

540 This does not have the form of a LUE model, because of the non-linear dependence on  $I_{abs}$ . However,  
 541 the apparent discrepancy between the non-linear light response observed at short time scales (sub-  
 542 daily) and the linear light response described by the empirical LUE model on longer time scales  
 543 (weekly to monthly) can be resolved if it is assumed  $J_{max}$  acclimates to  $I_{abs}$  over longer time scales. To  
 544 show this, we further assume that (a) there exists an optimal  $J_{max}$  for given average light conditions that  
 545 maximizes the differences between the benefit and cost of maintaining this value of  $J_{max}$ , which  
 546 conceptually includes the maintenance of light-harvesting complexes and the various proteins involved  
 547 in electron transport; (b) the benefit is the assimilation rate  $A$ , whereas the cost is the product of  $J_{max}$   
 548 and a parameter  $c$  (defined as the unit cost of maintaining  $J_{max}$ ); (c)  $V_{cmax}$  and  $J_{max}$  vary with

549 environmental conditions on a monthly time scale, while the unit costs  $b$  and  $c$  of maintaining  $V_{cmax}$  and  
 550  $J_{max}$  respectively are unchanged; and (d)  $V_{cmax}$  and  $J_{max}$  are related via the coordination hypothesis ( $A_c =$   
 551  $A_j = A$ ). The optimality criterion for  $J_{max}$  is then simply:

$$552 \quad \partial A / \partial J_{max} = c \quad (44)$$

553 Taking the partial derivative of  $A$  with respect to  $J_{max}$  in equation (43) leads to:

$$554 \quad c = \frac{\partial A}{\partial J_{max}} = \frac{m(\varphi_0 I_{abs})^3}{4 \sqrt{\left[ (\varphi_0 I_{abs})^2 + \left( \frac{J_{max}}{4} \right)^2 \right]^3}} \quad (45)$$

555 Equation (43) can now be rewritten as

$$556 \quad A = \varphi_0 I_{abs} m \sqrt{1 - \left( \frac{4c}{m} \right)^{\frac{2}{3}}} \quad (46)$$

557 This is a key algebraic result because  $A$  is now, once again, proportional to  $I_{abs}$ .

558 Next, applying the coordination hypothesis ( $A_c = A_j = A$ ):

$$559 \quad \frac{\varphi_0 I_{abs}}{\sqrt{\left( \varphi_0 I_{abs} \right)^2 + \left( \frac{J_{max}}{4} \right)^2}} = \frac{4V_{cmax}(c_i - \Gamma^*)}{J_{max}(c_i + K)m} \quad (47)$$

560 Substituting equation (47) into equation (45) and expanding the CO<sub>2</sub> limitation term  $m$ , we can express  
 561 equation (45) as:

$$562 \quad c = \frac{\partial A}{\partial J_{max}} = 16(c_i + 2\Gamma^*)^2 (c_i - \Gamma^*) \left( \frac{V_{cmax}}{J_{max}(c_i + K)} \right)^3 \quad (48)$$

563 Taking typical values of  $J_{max}/V_{cmax} = 1.88^{23}$  and  $\chi = 0.8^{46}$ , we estimate  $c = 0.103$  for standard conditions  
 564 ( $T = 25$  °C,  $z = 0$  km,  $c_a = 400$  ppm), leading to:

$$565 \quad A = \varphi_0 I_{abs} m \sqrt{1 - \left( \frac{c^*}{m} \right)^{\frac{2}{3}}} \quad (49)$$

566 where

567 
$$m = \frac{c_a - \Gamma^*}{c_a + 2\Gamma^* + 3\Gamma^* \sqrt{\frac{1.6D\eta^*}{\beta(K + \Gamma^*)}}} \quad (50)$$

568 and the constant  $c^*$  is 4 times  $c$ , the unit cost of maintaining  $J_{max}$ . As an indirect test of the assumptions,  
 569 the responses of  $J_{max}/V_{cmax}$  to temperature and CO<sub>2</sub> from equation (48) are compared with observations  
 570 (Supplementary Information).

571 A fuller derivation of  $\chi$ ,  $\chi_c$  and light-use efficiency model is provided in Supplementary Information.

### 572 **GPP data-model comparison**

573 Equations (2)-(3) yielded modelled site-specific monthly GPP values for comparison with values  
 574 independently derived from eddy-covariance measurements of CO<sub>2</sub> exchange in the Free and Fair Use  
 575 subset of the FLUXNET archive, using a consistent gap-filling procedure (Supplementary  
 576 Information). The monthly GPP data derived from flux measurements are archived in BitBucket (Data  
 577 link: <https://bitbucket.org/labprentice/gepisat/src/8d34456aafcd/results>) for public access. For the  
 578 modelled values, monthly LUE was estimated based on temperature and vapour pressure extracted  
 579 from CRU time-series (TS 3.22) data at 0.5° resolution<sup>47</sup> and site-observed  $c_a$ . Monthly absorbed PPF  
 580 was estimated as the product of PPF (0.45 times the WATCH incident surface shortwave radiation<sup>48</sup>,  
 581 divided by 0.22 J  $\mu\text{mol}^{-1}$ ) and the MODIS Enhanced Vegetation Index (EVI), equated to the fraction of  
 582 photosynthetically active radiation absorbed by foliage<sup>49</sup>. To match the WATCH data resolution,  
 583 wherever each site was located, EVI was upscaled from to the 0.5° grid cell based on the arithmetic  
 584 mean of the 100 valid 0.05° pixels within each pixel at the 0.5° resolution.

585 Data availability

586 The global carbon isotope dataset used here is available in GitHub with DOI:  
 587 10.5281/zenodo.569501<sup>17</sup>.

588

### 589 **References**

- 590 1 Ciais, P. *et al.* Carbon and other biogeochemical cycles. in *Climate change 2013: the physical*  
 591 *science basis. Contribution of Working Group I to the Fifth Assessment Report of the*  
 592 *Intergovernmental Panel on Climate Change* (eds Thomas F Stocker *et al.*) Ch. 6, 465-570  
 593 (Cambridge University Press, 2014).  
 594 2 Friedlingstein, P. *et al.* Uncertainties in CMIP5 climate projections due to carbon cycle  
 595 feedbacks. *Journal of Climate* **27**, 511-526 (2014).  
 596 3 Prentice, I. C., Liang, X., Medlyn, B. E. & Wang, Y. P. Reliable, robust and realistic: the three  
 597 R's of next-generation land-surface modelling. *Atmospheric Chemistry and Physics* **15**, 5987-  
 598 6005 (2015).

599 4 Wang, H., Prentice, I. C. & Davis, T. W. Biophysical constraints on gross primary production  
600 by the terrestrial biosphere. *Biogeosciences* **11**, 5987-6001 (2014).

601 5 Prentice, I. C., Dong, N., Gleason, S. M., Maire, V. & Wright, I. J. Balancing the costs of  
602 carbon gain and water transport: testing a new theoretical framework for plant functional  
603 ecology. *Ecology letters* **17**, 82-91 (2014).

604 6 Wright, I. J., Reich, P. B. & Westoby, M. Least - cost input mixtures of water and nitrogen for  
605 photosynthesis. *The American Naturalist* **161**, 98-111 (2003).

606 7 Monteith, J. L. Solar radiation and productivity in tropical ecosystems. *Journal of Applied*  
607 *Ecology* **9**, 747-766 (1972).

608 8 Farquhar, G. D., von Caemmerer, S. & Berry, J. A. A biochemical model of photosynthetic  
609 CO<sub>2</sub> assimilation in leaves of C<sub>3</sub> species. *Planta* **149**, 78-90 (1980).

610 9 Medlyn, B. E. Physiological basis of the light use efficiency model. *Tree Physiology* **18**, 167-  
611 176 (1998).

612 10 Ali, A. *et al.* A global scale mechanistic model of the photosynthetic capacity. *Geoscientific*  
613 *Model Development Discussions* **8**, 6217–6266 (2015).

614 11 Cai, W. *et al.* Large differences in terrestrial vegetation production derived from satellite-  
615 based light use efficiency models. *Remote Sensing* **6**, 8945-8965 (2014).

616 12 De Kauwe, M. G. *et al.* Forest water use and water use efficiency at elevated CO<sub>2</sub>: a model -  
617 data intercomparison at two contrasting temperate forest FACE sites. *Global Change Biology*  
618 **19**, 1759-1779 (2013).

619 13 Medlyn, B. E. *et al.* Reconciling the optimal and empirical approaches to modelling stomatal  
620 conductance. *Global Change Biology* **17**, 2134-2144 (2011).

621 14 Diefendorf, A. F., Mueller, K. E., Wing, S. L., Koch, P. L. & Freeman, K. H. Global patterns  
622 in leaf <sup>13</sup>C discrimination and implications for studies of past and future climate. *Proceedings*  
623 *of the National Academy of Sciences* **107**, 5738-5743 (2010).

624 15 Cowan, I. & Farquhar, G. Stomatal function in relation to leaf metabolism and environment.  
625 *Symposia of the Society for Experimental Biology*, 471-505 (1977).

626 16 Givnish, T. J. *On the Economy of Plant Form and Function*. Vol. 6 (Cambridge University  
627 Press, 1986).

628 17 Cornwell, W. K. *et al.* A global dataset of leaf  $\Delta^{13}\text{C}$  values. doi:10.5281/zenodo.569501  
629 (2017).

630 18 Farquhar, G. D., Ehleringer, J. R. & Hubick, K. T. Carbon isotope discrimination and  
631 photosynthesis. *Annual review of plant biology* **40**, 503-537 (1989).

632 19 Körner, C., Farquhar, G. & Wong, S. Carbon isotope discrimination by plants follows  
633 latitudinal and altitudinal trends. *Oecologia* **88**, 30-40 (1991).

634 20 Lin, Y.-S. *et al.* Optimal stomatal behaviour around the world. *Nature Climate Change* **5**,  
635 459–464 (2015).

636 21 Maire, V. *et al.* The coordination of leaf photosynthesis links C and N fluxes in C<sub>3</sub> plant  
637 species. *PloS one* **7**, e38345 (2012).



- 638 22 Haxeltine, A. & Prentice, I. C. A general model for the light-use efficiency of primary  
639 production. *Funct. Ecol.* **10**, 551-561, doi:10.2307/2390165 (1996).
- 640 23 Kattge, J. & Knorr, W. Temperature acclimation in a biochemical model of photosynthesis: a  
641 reanalysis of data from 36 species. *Plant, cell & environment* **30**, 1176-1190 (2007).
- 642 24 Collatz, G., Berry, J., Farquhar, G. & Pierce, J. The relationship between the Rubisco reaction  
643 mechanism and models of photosynthesis. *Plant, Cell & Environment* **13**, 219-225 (1990).
- 644 25 Beer, C. *et al.* Terrestrial gross carbon dioxide uptake: global distribution and covariation with  
645 climate. *Science* **329**, 834-838 (2010).
- 646 26 Yuan, W. *et al.* Global comparison of light use efficiency models for simulating terrestrial  
647 vegetation gross primary production based on the LaThuile database. *Agricultural and forest  
648 meteorology* **192**, 108-120 (2014).
- 649 27 Ainsworth, E. A. & Long, S. P. What have we learned from 15 years of free - air CO<sub>2</sub>  
650 enrichment (FACE)? A meta - analytic review of the responses of photosynthesis, canopy  
651 properties and plant production to rising CO<sub>2</sub>. *New Phytologist* **165**, 351-372 (2005).
- 652 28 Frank, D. C. *et al.* Water-use efficiency and transpiration across European forests during the  
653 Anthropocene. *Nature Climate Change* **5**, 579-583 (2015).
- 654 29 Maire, V. *et al.* Global effects of soil and climate on leaf photosynthetic traits and rates.  
655 *Global Ecology and Biogeography* **24**, 706-717 (2015).
- 656 30 Kaplan, J. O. Geophysical applications of vegetation modeling. (Lund University, 2001).
- 657 31 Chen, J.-L., Reynolds, J. F., Harley, P. C. & Tenhunen, J. D. Coordination theory of leaf  
658 nitrogen distribution in a canopy. *Oecologia* **93**, 63-69 (1993).
- 659 32 Vogel, H. Temperaturabhängigkeitsgesetz der Viskosität von Flüssigkeiten. *Physik Z* **22**, 645-  
660 646 (1921).
- 661 33 Jacob, D. *Introduction to atmospheric chemistry.* (Princeton University Press, 1999).
- 662 34 Bernacchi, C. J., Singsaas, E. L., Pimentel, C., Portis Jr, A. R. & Long, S. P. Improved  
663 temperature response functions for models of Rubisco - limited photosynthesis. *Plant, Cell &  
664 Environment* **24**, 253-259 (2001).
- 665 35 New, M., Lister, D., Hulme, M. & Makin, I. A high-resolution data set of surface climate over  
666 global land areas. *Climate research* **21**, 1-25 (2002).
- 667 36 Keenan, T. F., Sabate, S. & Gracia, C. Soil water stress and coupled photosynthesis-  
668 conductance models: Bridging the gap between conflicting reports on the relative roles of  
669 stomatal, mesophyll conductance and biochemical limitations to photosynthesis. *Agricultural  
670 and Forest Meteorology* **150**, 443-453 (2010).
- 671 37 Sun, Y. *et al.* Impact of mesophyll diffusion on estimated global land CO<sub>2</sub> fertilization.  
672 *Proceedings of the National Academy of Sciences* **111**, 15774-15779 (2014).
- 673 38 Flexas, J., Ribas - Carbo, M., DIAZ - ESPEJO, A., GalmES, J. & Medrano, H. Mesophyll  
674 conductance to CO<sub>2</sub>: current knowledge and future prospects. *Plant, Cell & Environment* **31**,  
675 602-621 (2008).

676 39 Gu, J., Yin, X., Stomph, T.-J., Wang, H. & Struik, P. C. Physiological basis of genetic  
677 variation in leaf photosynthesis among rice (*Oryza sativa* L.) introgression lines under drought  
678 and well-watered conditions. *Journal of experimental botany* **63**, 5137-5153 (2012).

679 40 Douthe, C., Dreyer, E., Epron, D. & Warren, C. Mesophyll conductance to CO<sub>2</sub>, assessed  
680 from online TDL-AS records of <sup>13</sup>CO<sub>2</sub> discrimination, displays small but significant short-  
681 term responses to CO<sub>2</sub> and irradiance in *Eucalyptus* seedlings. *Journal of Experimental*  
682 *Botany* **62**, 5335-5346 (2011).

683 41 Barbour, M., Warren, C., Farquhar, G., Forrester, G. & Brown, H. Variability in mesophyll  
684 conductance between barley genotypes, and effects on transpiration efficiency and carbon  
685 isotope discrimination. *Plant, Cell & Environment* **33** (2010).

686 42 Ubierna, N. & Farquhar, G. D. Advances in measurements and models of photosynthetic  
687 carbon isotope discrimination in C<sub>3</sub> plants. *Plant, cell & environment* **37**, 1494-1498 (2014).

688 43 Warren, C. R. Stand aside stomata, another actor deserves centre stage: the forgotten role of  
689 the internal conductance to CO<sub>2</sub> transfer. *Journal of Experimental Botany* **59**, 1475-1487  
690 (2008).

691 44 Smith, E. L. The influence of light and carbon dioxide on photosynthesis. *The Journal of*  
692 *general physiology* **20**, 807-830 (1937).

693 45 Harley, P. C., Thomas, R. B., Reynolds, J. F. & Strain, B. R. Modelling photosynthesis of  
694 cotton grown in elevated CO<sub>2</sub>. *Plant, Cell & Environment* **15**, 271-282 (1992).

695 46 Lloyd, J. & Farquhar, G. D. <sup>13</sup>C discrimination during CO<sub>2</sub> assimilation by the terrestrial  
696 biosphere. *Oecologia* **99**, 201-215 (1994).

697 47 Harris, I., Jones, P., Osborn, T. & Lister, D. Updated high-resolution grids of monthly climatic  
698 observations—the CRU TS3.10 Dataset. *International Journal of Climatology* **34**, 623-642  
699 (2014).

700 48 Weedon, G. P. *et al.* The WFDEI meteorological forcing data set: WATCH Forcing Data  
701 methodology applied to ERA-Interim reanalysis data. *Water Resources Research* **50**, 7505-  
702 7514 (2014).

703 49 Xiao, X., Zhang, Q., Hollinger, D., Aber, J. & Moore, B. I. Modeling gross primary  
704 production of an evergreen needleleaf forest using MODIS and climate data. *Ecol. Appl.* **15**,  
705 954-969 (2005).

706

